

Development of a Laser Micro-Thruster and On-Orbit Testing

Jifei Ye ¹ , Sibowang Wang ^{2,*}, Hao Chang ^{1,*}, Yanji Hong ¹, Nanlei Li ¹, Weijing Zhou ¹, Baoyu Xing ¹, Bangdeng Du ¹ and Chengyin Xie ³

¹ State Key Laboratory of Laser Propulsion & Application, Space Engineering University, Beijing 101416, China; yjf1981@163.com (J.Y.); hongyanji@vip.sina.com (Y.H.); 15910624233@163.com (N.L.); bddu13s@alum.imr.ac.cn (B.D.)

² Beijing Institute of Tracking and Telecommunications Technology, Beijing 100094, China

³ Spacety Co., Ltd., Changsha 410221, China; xiechengyin@spacety.cn

* Correspondence: bosiwang1@163.com (S.W.); changhao5976911@163.com (H.C.)

Abstract: Laser micro-thrust technology is a type of propulsion that uses a laser beam to ablate a propellant such as a metal or plastic. The ablated material is expelled out the back of the spacecraft, generating thrust. The technology has the advantages of high control precision, high thrust–power ratios, and excellent performances, and it has played an important role in the field of micro-propulsion. In this study, a solid propellant laser micro-thruster was developed and then applied for the attitude control of satellites during on-orbit tests. The micro-thruster had a volume of 0.5 U, a weight of 440 g, and a thrust range of 10 μ N–0.6 mN. The propellant, 87% glycidyl azide polymer (GAP) + 10% ammonium perchlorate (AP) + 3% carbon nano-powder, was supplied via a double-layer belt, and the average power was less than 10 W. We present the development of the laser micro-thruster, as well as the results regarding the thruster propulsion performance. The thruster was launched into orbit on 27 February 2022 with the Chuangxin Leishen Satellite developed by Spacety. The on-orbit test of the thruster for satellite attitude control was carried out. The thruster was successfully fired in space and played an obvious role in the attitude control of the satellite. The experimental results show that the thrust is about 315 μ N.

Keywords: laser micro-thruster; micro- and nano-satellites; thrust; on-orbit test; attitude control



Citation: Ye, J.; Wang, S.; Chang, H.; Hong, Y.; Li, N.; Zhou, W.; Xing, B.; Du, B.; Xie, C. Development of a Laser Micro-Thruster and On-Orbit Testing. *Aerospace* **2024**, *11*, 23. <https://doi.org/10.3390/aerospace11010023>

Academic Editor: John Sinko

Received: 28 September 2023

Revised: 6 December 2023

Accepted: 23 December 2023

Published: 26 December 2023



Copyright: © 2023 by the authors. Licensee MDPI, Basel, Switzerland. This article is an open access article distributed under the terms and conditions of the Creative Commons Attribution (CC BY) license (<https://creativecommons.org/licenses/by/4.0/>).

1. Introduction

In recent years, satellites have gradually developed toward miniaturization and integration. Micro- and nano-satellites have small sizes and low manufacturing costs [1] and are suitable for mass production and application. Hence, they are playing an increasingly important role in many fields [2,3]. However, the development of satellite propulsion technology has greatly lagged behind other technologies used in micro- and nano-satellites. With the increase in demand for orbit maintenance, formation networking, and maneuvering of micro- and nano-satellites, there has been more and more attention on the development of propulsion technologies for attitude and orbit control.

Micro- and nano-satellites require precise, controllable, and continuous thrust output in order to achieve orbit change [4], attitude control [5], and rapid maneuvering [6]. Laser micro-thrust technology is an important type of propulsion technology. The principle of laser micro-thrust technology is that a laser beam from the thruster ablates the propellant, and the ablated material is ejected to generate propulsion. Laser micro-thrust technology has high specific impulses, high control precision, and low power consumption [7–10] and has, thus, attracted extensive attention.

Research on laser micro-propulsion technology emerged in the 1990s. Phipps et al. [11,12] first proposed the concept of laser ablation micro-propulsion. With the development of theory and method, a large number of laser micro-propulsion experiments using metals, non-metals, and polymers have been carried out, which have improved our understanding of the technology.

There have been more and more studies on practical engineering applications of laser micro-thrusters. The laser micro-thruster designed by Phipps's team [13,14] went through seven iterations from 2002 to 2008, and the performance was gradually improved. Moreover, various laser micro-thrusters that operated at the ms, μ s, and ns scales were designed and tested, yet so far, there have been no reports of on-orbit applications of these micro-thrusters.

In 2005, Koizumi et al. [15] invented a dual-mode laser micro-thruster that operated via ablation mode and ignition mode. The propellant used in the ablation mode was customized polyvinyl chloride PVC + 5% carbon powder. By changing the laser pulse width, the impulse of a single pulse could be precisely controlled between 1 and 40 μ N·s. In the ignition mode, the propellant used was the potassium boron nitrate series propellant B/KNO₃, and a single pulse could generate an average impulse of 11 mN·s. This dual-mode design enabled the laser micro-thruster to achieve thrusts in a range spanning four orders of magnitude (0.1 μ N–10 mN).

On 23 January 2009, Japan simultaneously launched seven satellites, one of which, named KKS-1, is equipped with a laser micro-thruster [16]. The satellite has a weight of 3.1 kg and a volume of 1.5 U. It uses a dual-mode design to achieve propulsion, and laser micro-thruster and flywheels are used for three-axis satellite attitude control. The thruster uses a semiconductor laser with a wavelength of 808 nm. Due to a malfunction of the on-board CPU, resulting in a communication interruption, the experiment of attitude control was not carried out.

Baumanets Moscow State Technical University (BMSTU) proposed the "Baumanets-2" program in 2010, and the laser micro-thruster LDU-7 is the important test load of the satellite. The LDU-7 laser micro-thruster has dimensions of 162 × 88 × 76 mm, a mass of 0.9 kg, and a design life of 1 year. It is powered through a 12 or 27 V on-board power supply. The propellant of LDU-7 is polytetrafluoroethylene doped with carbon powder, which is irradiated with light by a 10 W fiber-coupled semiconductor laser with a wavelength of 808 nm and a spot diameter of 300 μ m. The total designed impulse of LDU-7 is 4 N·s, the impulse of a single pulse can be changed by adjusting the laser power density and pulse width, and the minimum impulse is 10⁻⁶ N·s. The maximum working frequency is 100 Hz. With a 10 W power consumption and 50 ms pulse width, the average thrust is about 4 mN, and the impulse coupling coefficient is 4 × 10⁻⁴ N/W. The "Baumanets-2" satellite was launched on 28 November 2017 on board the Soyuz 2.1B rocket [17]. Unfortunately, the satellites carried by the Soyuz 2.1B rocket crashed into the Atlantic Ocean due to the failure of the rocket's Fregat upper stage after reaching the 196 km apogee non-closed orbit [18].

On 27 July 2022, a laser micro-propulsion system designed by Cai et al. [19] was successfully launched into orbit. The thrusters are used for ultra-precise orbit and attitude control. However, there has been no report on the performance of the thruster so far. In the past two decades, the field of laser micro-propulsion and its engineering applications have seen great development. Many teams have attempted on-orbit tests. However, there is still no successful on-orbit verification of laser micro-thrusters.

In this study, we developed a laser micro-thruster with a solid propellant. The thruster, named SLP-1K, uses multiple semiconductor lasers. Propulsion is achieved through ablation of the multi-layer solid propellant. It was launched into orbit by the Long March 8 carrier rocket at the Wenchang Space Launch Site in China on 27 February 2022, on board the TY22 Chuangxin Leishen satellite. The orbital altitude was 500 km. After entering orbit, the performance of SLP-1K was tested on-orbit in September 2022, and we obtained on-orbit test data of the laser micro-thruster for the first time, which demonstrated the feasibility of the laser micro-thruster for attitude control of micro- and nano-satellites.

2. Development of SLP-1K

2.1. Design

The SLP-1K laser micro-thruster is primarily composed of three parts: a laser source and optical components for shaping and focusing; storage and supply systems for the propellant; and electronic components for control and energy supply. The operation is

as follows: The satellite platform sends signals, and the thruster's control unit receives them. Then, the control unit sends signals to the laser components and the propellant supply system such that the propellant is translated at a specific speed, enabling a stable ablation process. SLP-1K uses laser beams emitted by laser diodes with fiber output to irradiate the strip-shaped thin-film energetic solid propellant, and the laser ablation plume is ejected from the surface of the target at a high speed, thereby achieving propulsion. By changing the ablation frequency (the laser pulse frequency), different thrust levels can then be achieved.

The volume of SLP-1K is 0.5 U (100 mm × 100 mm × 50 mm), and the weight is 440 g. The thruster is shown in Figure 1. The schematic depicting the diode laser configuration, propellant feed system, power processing unit, and controller are shown in Figure 2. The operating temperature of the thruster is −25 to 50 °C, the storage temperature is −50 to 80 °C, and the expected life of the satellite is 1 year.

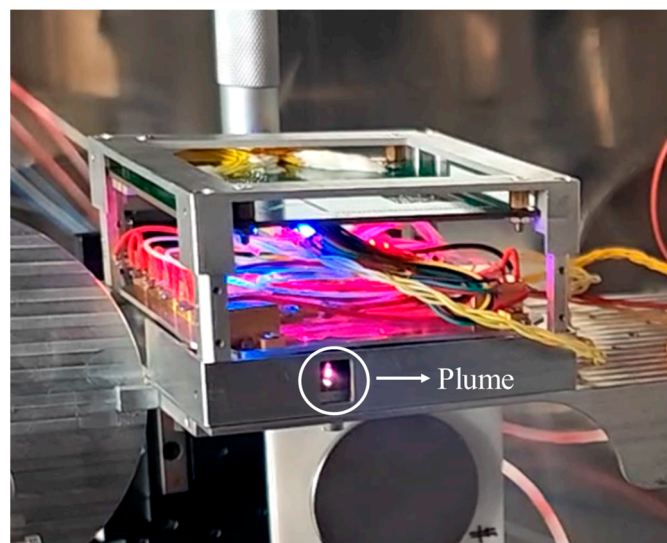


Figure 1. A photograph of the laser micro-thruster.

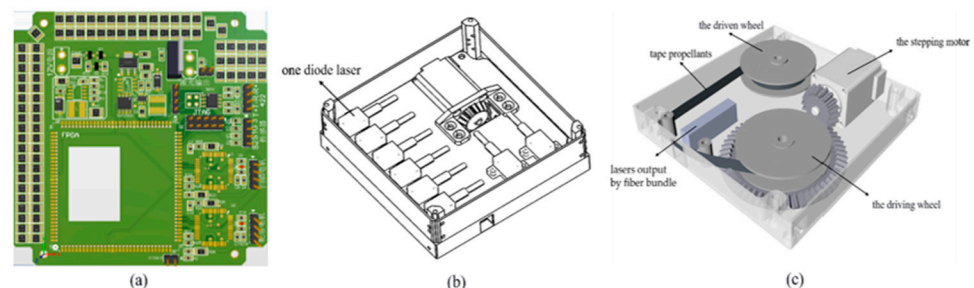


Figure 2. Details of the thruster: (a) power processing unit and controller, (b) diode laser configuration, and (c) propellant feed system.

SLP-1K uses laser diodes to ablate the solid propellant. The thrust contains a total of eight lasers. The laser beam is coupled with the optical fiber through the FC interface which is at the end of each diode laser. A fiber-coupled output of eight-diode-laser array is designed in order to achieve a high ablation effect. Each fiber-coupled output is arranged side by side, and the distance between them is 714 μm . The maximum output power of a single diode laser is 10 W; the wavelength is 940 nm; the output fiber core diameter is 105 μm ; the numerical aperture is 0.22; and the power density of the focused spot is more than 10^5 W/cm^2 . The laser can work at 100 μs ~1 ms pulse width, and the highest pulse frequency is 50 Hz.

The ablation mode is used by SLP-1K, and the propellant is delivered using a belt with two layers. The bottom layer is a transparent base made of polyethylene terephthalate (PET) with good light transmittance (95%), high tensile strength, and high temperature resistance. The component of the ablative layer is mainly GAP (87%) with 10% AP in order to achieve an oxygen balance and 3% carbon nano-powder to improve the laser absorption rate of the propellant. The initial thickness of the PET layer was about 100 μm , and that of the ablative layer was about 200 μm . Once the laser ablates the top layer, the ablated material was blocked by the transparent layer and ejected out. This design avoids the contamination of optical devices. To make the belt, plasma was first used to treat the PET, and then a GAP solution was applied to the PET. Plasma processing effectively increases the binding force and avoids peeling due to ablation, thereby producing a stable impulse [20]. Figure 3 shows a schematic diagram of the double-layer belt.

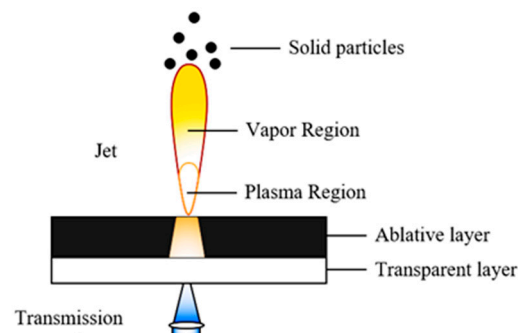


Figure 3. Schematic diagram of laser ablation.

2.2. Propulsion Performance of Thruster

2.2.1. Measuring Equipment and Principles

The propulsion performance of a micro-thruster is usually characterized by the size, accuracy, and dynamic adjustability of the thrust. In this study, the impulse and average thrust were measured based on the torsional pendulum method. The measurement of the thrust was carried out using a customized platform (Figure 4). The platform was designed based on the torsional pendulum principle. It was composed of a test platform, beam, thruster, and signal acquisition and storage unit. The 12 V battery was attached to the beam, and wireless communication was used to avoid external interference. Under the action of thrust and impulse, the beam rotates around the shaft, and the flexural pivot at both ends of the shaft generate a restoring moment. By measuring the swing displacement of the beam, the thrust can be calculated.

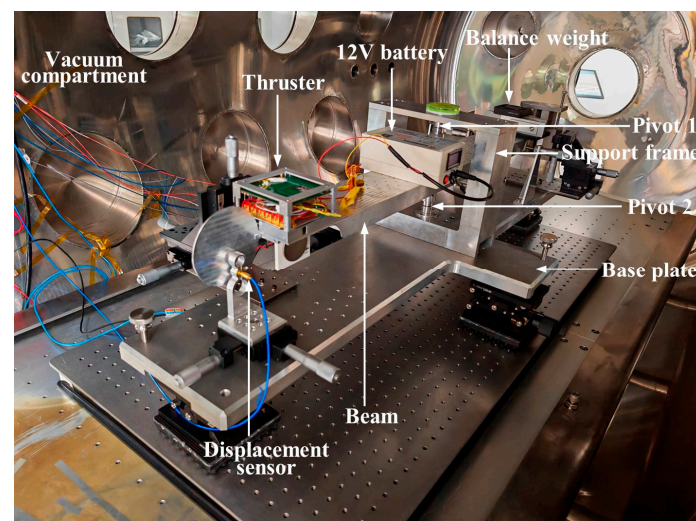


Figure 4. Average thrust measurement device.

A single-pulse laser ablates the material on the torsional pendulum. After the propellant is ablated, gasification and ionization occur, and jets are formed to generate a reaction force, thereby pushing the torsional pendulum to move to a certain angle. A second-order equation results in damped vibrations. Then, the displacement sensor is used to record the relative position of the torsional pendulum at a high sampling rate. The magnitude of the single impulse is then calculated based on the difference between the maximum displacement and the equilibrium position of the pendulum.

During laser ablation, the torsional pendulum is mainly subject to two moments, a restoring moment from the pivot and a rotational moment from the ejection of the ablated materials. It is assumed that J is the moment of inertia of the entire system, c is the damping coefficient, k is the stiffness coefficient of the pivot, and θ is the deflection angle; then the angular velocity is $\dot{\theta}$, the angular acceleration is $\ddot{\theta}$, and d is the distance between the laser spot and the center of the pivot. The external force at time t is $f(t)$. T_0 is the action time of the external force. Then, the motion of the pendulum is expressed as

$$\begin{cases} J\ddot{\theta} + c\dot{\theta} + k\theta = f(t)d & 0 < t < T_0 \\ J\ddot{\theta} + c\dot{\theta} + k\theta = 0 & t > T_0 \end{cases} \quad (1)$$

This can be changed to

$$\begin{aligned} \ddot{\theta} + 2\zeta\omega_n\dot{\theta} + \omega_n^2\theta &= f(t)d/J & 0 < t < T_0 \\ \omega_n &= \sqrt{\frac{k}{J}} & \zeta &= \frac{c}{2\sqrt{kJ}} \end{aligned} \quad (2)$$

where ζ is the damping ratio of the torsional pendulum system, and ω_n is the natural oscillation frequency.

When measuring impulse, it is assumed that the impulse is instantly loaded. In this case, the laser pulse width needs to be less than $1/12.8$ of the pendulum's oscillation period to allow for accurate measurement (the relative error is less than 1%) [21]. The typical torsion period is about 8 s, and the pulse thrust loading time is not more than 0.625 s, which can be considered as instantaneous impulse coupling. At this point, the dynamic equation for the impact of instantaneous coupled pulse impulse $I\delta(t)$ (where $\delta(t)$ is the Dirac distribution function) on a torsional pendulum is

$$\ddot{\theta} + 2\zeta\omega_n\dot{\theta} + \omega_n^2\theta = I\delta(t)d/J \quad (3)$$

The solution of the equation is

$$\theta(t) = \frac{Id}{J\omega_d} e^{-\zeta\omega_n t} \sin \omega_d t \quad (4)$$

where $\omega_d = \sqrt{1 - \zeta^2}\omega_n$ is the actual vibration frequency.

According to Equation (4), the deflection angle θ is a function of time. To obtain the single impulse, the constants d , ω_d , J , and ζ are needed. Taking the derivative of this equation, the maximum value of the deflection angle of the torsion pendulum is

$$\theta_{\max} = \frac{Id}{J\omega_n} e^{-\frac{\zeta}{\sqrt{1-\zeta^2}} \arctan \frac{\sqrt{1-\zeta^2}}{\zeta}} \quad (5)$$

By applying standard force and calibrating the parameters of the torsion pendulum, the obtained result is $d = 0.3915 \pm 0.0001$ m, $k = 0.191 \pm 0.001$ Nm/rad, $J = 0.308 \pm 0.006$ kg·m², $\zeta = 0.179 \pm 0.002$. Specifically, due to the small damping ratio, the exponential term of e is

approximately 1, which means the influence of the damping ratio can be ignored. Then, the relationship between the maximum torsion angle and the single impulse is rewritten as

$$\theta_{\max} = \frac{Id}{J\omega_n} \quad (6)$$

Obviously, the maximum amplitude position reached by the first oscillation of a torsion pendulum after being subjected to instantaneous impulse corresponds to θ_{\max} . In the actual measurement process, the small angle assumption is used to convert angle measurement into linear displacement measurement at a certain measuring point, and then combined with the calibrated torsion pendulum parameters, the impulse is measured. According to the standard deviation transfer relationship of various calibration parameters, it can be determined that the uncertainty of the impulse measurement range of the torsion pendulum is better than 95% in the range of 10 $\mu\text{N}\cdot\text{s}$ ~500 $\mu\text{N}\cdot\text{s}$.

When measuring thrust, it is considered as the steady-state average thrust. In this case, the torsion pendulum is subjected to a constant force F , which can be regarded as the superposition of a series of pulse excitations, and the system response under the constant force can be obtained through the principle of linear superposition. Within a small time interval of $t = \tau$ to $\tau + d\tau$, the pulse impulse generated by constant force is $Fd\tau$. According to the superposition principle of linear systems, it can be obtained that the response of the system under constant force F is equal to the sum of the pulse responses of the system within $0 \leq \tau \leq t$. That is to say,

$$\begin{aligned} \theta(t) &= \int_0^t dIh(t-\tau)Fd\tau \\ &= \frac{dF}{k} \left(1 - \frac{1}{k\sqrt{1-\zeta^2}} e^{-\zeta\omega_n t} \sin(\omega_d t + \phi) \right) \end{aligned} \quad (7)$$

where $h(t)$ is the impulse response function,

$$\tan \phi = \sqrt{1 - \zeta^2} / \zeta \quad (8)$$

When time approaches infinity, the steady-state response under constant force can be simplified as

$$\lim_{t \rightarrow \infty} \theta(t) = \theta(\infty) = \frac{dF}{k} \quad (9)$$

After obtaining the steady-state system response under constant force through measurement, the magnitude of the applied constant force can be obtained according to the above equation.

$$F = \frac{k\theta(\infty)}{d} \quad (10)$$

Similarly, under the assumption of small angles, the relationship between the line displacement P can be obtained from a line displacement measurement point with a distance of l from the axis of rotation, and the deflection angle is $P = \theta(\infty)l$. Therefore, based on the calibration results of the torsion pendulum parameters, the magnitude of the measured thrust can be calculated by measuring the swing line displacement at a certain measuring point on the torsion pendulum (l set to 0.5 m).

The thrust F is calculated as follows:

$$F = \frac{k}{dl} P \quad (11)$$

Since d , l , and k are all constants, the linear relationship between the thrust F and the linear displacement P can be determined. The range of the thrust measurement platform was 2 μN ~350 μN , and the measurement accuracy was higher than 97%.

2.2.2. Thrust Performance of the Laser Micro-Thruster

In order to verify the accuracy and repeatability of the thruster impulse, the total impulse under different pulse numbers is measured. The total impulse of the thruster changes with the number of pulses, as shown in Figure 5. The pulse width of the laser is set to 900 μs . As the number of laser pulses increases from 10 to 30, the total impulse increases from 31.44 $\mu\text{N}\cdot\text{s}$ to 100.74 $\mu\text{N}\cdot\text{s}$. Through linear fitting, it can be seen that the total impulse is approximately linear with the change in the number of pulses.

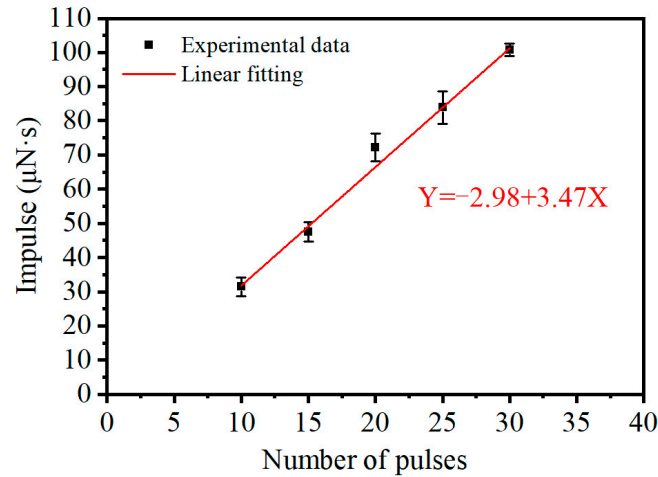


Figure 5. The relationship between the total impulse and the number of pulses.

The pulse width of the laser has great influence on the performance of the thruster. The total impulse of the thruster varies with the pulse width of the laser, as shown in Figure 6, where the number of pulses is set to 20. It can be seen that as the laser pulse width increases from 100 μs to 900 μs , the total impulse increases approximately linearly from 58.52 $\mu\text{N}\cdot\text{s}$ to 72.24 $\mu\text{N}\cdot\text{s}$.

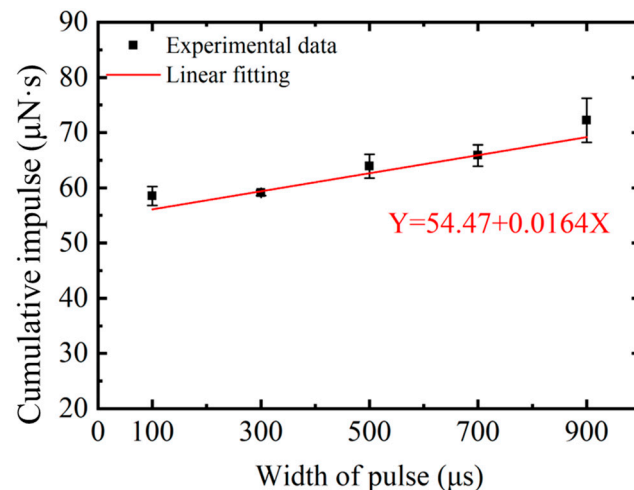


Figure 6. The total impulse of the thruster varies with the pulse width of the laser.

Table 1 shows the power consumption parameters of the thruster in four different modes. From the results, it can be observed that with the increase in the thrust, the thrust–power ratio gradually increased. A maximum thrust–power ratio of 45.82 $\mu\text{N}/\text{W}$ was reached under a thrust of 300 μN .

Table 1. Performance of SLP-1K under four modes.

Thrust (μN)	Total Power Consumption (W)	Thrust–Power Ratio ($\mu\text{N/W}$)
10	2.07	4.84
150	3.95	37.96
200	5.02	39.88
300	6.55	45.82

3. Mechanical Tests

Assessment of the environmental adaptability of SLP-1K is essential for a successful mission. In order to test the reliability, stability, and adaptability of the laser micro-thruster in the space environment, we carried out relevant assessments in this study.

3.1. Mechanical Tests

The purpose of the mechanical test was to evaluate the structural strength of SLP-1K and the reliability of the components. In order to prevent damage to the thruster, a customized fixture was designed, and then the thruster and the fixture were placed on the vibration test bench. The range of frequencies in the test was at the qualification level, i.e., the highest level of mechanical testing. The test conditions are shown in Tables 2–4.

Table 2. Sinusoidal vibration test.

Frequency Range	Vibration Amplitude
	Qualification Level
10~20 Hz	10 mm (0–P)
20~100 Hz	16 g
Scan rate	2 oct/min
Loading direction	Three axial directions

Table 3. Random vibration test.

Frequency Range	Power Spectral Density
	Qualification Level
10~100 Hz	+6 dB/oct
100~800 Hz	0.25 g^2/Hz
800~2000 Hz	–15 dB/oct
Total RMS	2 oct/min
Loading time	2 min
Loading direction	Three axial directions

Table 4. Shock response test ($Q = 10$).

Frequency Range	Qualification Level
100~600 Hz	+6 dB/oct
600~4000 Hz	1000 g
Loading time	2 times
Loading direction	Three axial directions

3.2. Low-Pressure Discharge Test

Low-pressure discharges; corona and arc discharge phenomena; or high-voltage micro-discharges can occur in the components at the power-on stage of the active section and the

initial orbital phase. The test pressure changed from normal ambient pressure to 1.3 Pa gradually; the laboratory ambient temperature was 23–24 °C; and the humidity was 33–38% RH. The half cycle time was 10 min, and three tests were performed. It was found that there were no abnormal phenomena, such as arc discharges and coronas.

3.3. Vacuum Thermal Cycling Test

To verify the adaptability of SLP-1K to high and low temperatures under vacuum conditions, a vacuum thermal cycling test was carried out, and the laser output capability was verified. The thermal cycling test conditions were as follows: The ambient pressure was less than 1.3×10^{-3} Pa, and the temperature was -20 °C to $+100$ °C. The temperature was cycled three times from room temperature to $+50$ °C and then three times from room temperature to $+80$ °C. Finally, a temperature limit test was carried out. Specifically, the temperature was first lowered to -20 °C, and then the temperature gradually rose to 100 °C. Each temperature level was held for 2 h in each cycle. The temperature sensor was placed on the external surface of the component to ensure that the measured value was the temperature of the component.

3.4. Electromagnetic Compatibility Test

The conduction emission of the power input of the whole thruster was measured. In order to detect whether the electric field emission from the laser micro-thruster exceeded the specified requirements, the laser micro-thruster was placed on a platform in a shielded dark room. At a distance of 1 m from the device being tested, a source rod antenna, biconical antenna, and double-ridge horn antenna were set up. The two polarization modes of the antennas were measured above 30 MHz, and the field radiation was monitored.

It was found that the conduction emission amplitude of the power input and power return line of the laser micro-thruster was lower than the limit, and the thruster passed the CE102 power line conduction emission test. In the electric field radiation emission test, the laser micro-thruster had an over-standard point in the 10 kHz–30 MHz frequency band. The over-standard frequency was 622.5 kHz, and the amplitude was 45.15 dBuV/m, which was 3.23 dBuV/m above the limit. The over-frequency phenomenon could be avoided by wrapping the thruster with a shielding layer.

4. On-Orbit Test of SLP-1K

Figure 7 shows the TY22 Chuangxin Leishen satellite. It has a volume of 6 U and a weight of 10 kg. The SLP-1K micro-thruster was used as a test load and installed at one end of the satellite to facilitate attitude control. The red circle showed the location of the thruster. The X-axis moment of the thruster was $9.5 \mu\text{N}\cdot\text{m}$.



Figure 7. TY22 Chuangxin Leishen satellite.

In this study, the satellite body and flywheel were considered to be one body, and the angular momentum was conserved when there were no external moments. The spatial disturbance moment and the angular momentum produced by other rotatable parts on

the satellite were all external moments for the satellite–flywheel system. In the inertial mode, the three angular velocities of the satellite were kept at 0, and the effect of external moments on the satellite–flywheel system could be reflected by changing the rotational speed of the flywheel.

The possible external moments in the test included the spatial disturbance moments (aerodynamic moments, solar pressure moments, gravity gradient moments, and geomagnetic moments), moments generated by the rotor of the laser micro-thruster, and moments generated due to the moment arm of the thrust axis relative to the spacecraft CG. The first step of the test was to determine the spatial disturbance moment of the satellite in the inertial mode, that is, to measure the change in the rotational speed of the flywheel when the laser micro-thruster was not operating.

The conversion between the rotational speed and angular momentum is described as follows. Suppose the rotational speed is $[x \ y \ z \ s]^T$. The flywheel installation matrix (direction cosine matrix) is $C = \begin{bmatrix} xx' & yx' & zx' & sx' \\ xy' & yy' & zy' & sy' \\ xz' & yz' & zz' & sz' \end{bmatrix}$, representing the positional relationship between the flywheel and the satellite. The angular momentum of the four flywheels in the satellite coordinate system H_{wheel} is calculated as follows:

$$H_{\text{wheel}} = C \times [x \ y \ z \ s]^T \times I_{\text{wheel}} \times (2\pi/60) \quad (12)$$

x_{speed} , y_{speed} , z_{speed} , and s_{speed} are the rotational speeds of the flywheels along the x , y , z , and s axes, respectively, and C is the installation matrix of the flywheel:

$$C = \begin{bmatrix} -1 & 0 & 0 & -0.57729 \\ 0 & 1 & 0 & 0.57729 \\ 0 & 0 & 1 & 0.57729 \end{bmatrix}$$

I_{wheel} is the moment of inertia of the flywheel, which is 0.000006095 kg·m².

The formula for the angular momentum of the satellite H_{sat} is as follows:

$$H_{\text{sat}} = I_{\text{sat}} \times [w_x \ w_y \ w_z]^T \quad (13)$$

where I_{sat} is the moment of inertia of the satellite; and ω_x , ω_y , and ω_z are the angular velocities of the satellite relative to the inertial system; and the moment of inertia of the satellite is

$$I_{\text{sat}} = \begin{bmatrix} 0.183687 & -0.000552 & 0.000058 \\ -0.000552 & 0.389528 & 0.004162 \\ 0.000058 & 0.004162 & 0.463517 \end{bmatrix}$$

The angular momentum of the flywheel–satellite system H_{total} is as follows:

$$H_{\text{total}} = H_{\text{wheel}} + H_{\text{sat}} \quad (14)$$

The relationship between the moment and angular momentum is as follows:

$$M = \frac{dH}{dt} \quad (15)$$

where M is the moment, H is the angular momentum, and t is time. Equation (11) shows whole star when the laser micro-thruster is operating into the above formula, and the ex that the derivative of the angular momentum with respect to time is the sum of external moments of the flywheel–satellite system. The angular momentum of the flywheel–nano-satellite system can be obtained by inserting the flywheel speed and the angular velocity of the nano-satellite when the laser micro-thruster is operating into the above formula, and the external moment of the system can be obtained by deriving the angular momentum with respect to time.

Figure 8 shows the rotational speeds of the x-axis flywheels. Figure 8a shows the rotational speeds of the flywheels when SLP-1K was not operating, and Figure 8b shows the speeds of the flywheels after SLP-1K was turned on. From the two graphs, it can be found that when the thruster was off, there were some oscillation changes in the flywheel speed, and the slope change in its average value is slight. The reason for the slight change is perhaps attributed to the spatial disturbance moments. When the thruster was turned on, the rotational speeds of the flywheels changed significantly, indicating a significant effect of the thruster. The total angular momentum of the system can be further obtained according to the speed of the flywheel, as shown in Figure 9. The thrust outputs were calculated based on the fitting coefficients. The x-axis thrust was about 315 μN . From the experimental results, it can be seen that the average thrust of the laser micro-thruster on orbits was higher than that of the ground experiments. The possible reason is the additional torque produced by the thruster. When the laser thruster is working, the rotations of the driving wheel and the driven one, which are used in the propellant feed system, bring some additional torques. Those torques will increase the attitude changes besides the net thrust produced by the thruster, eventually leading to a larger on-orbit thrust. However, in the ground test, the torsion pendulum system was used to measure the thrust perpendicular to the nozzle direction of the thruster, so the rotation torques in the thruster did not affect its thrust value. Therefore, the on-orbit thrust is higher than the ground one.

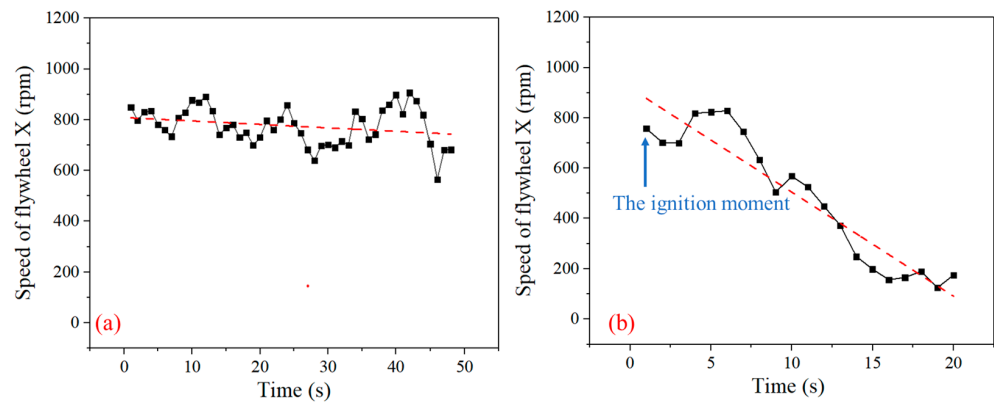


Figure 8. Presents the rotational speed of the satellite flywheels: speeds of flywheels along the x axis when the thruster was (a) off and (b) on. The black square in figure represents the speeds of flywheels along the x axis. The red dotted line represents the fitting line of the X-axis to the flywheel speed.

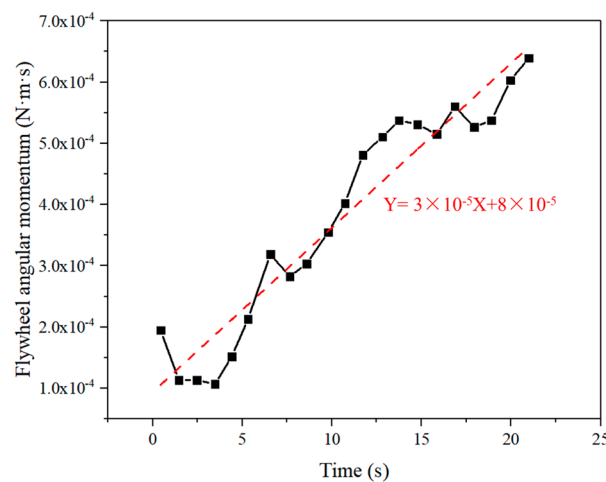


Figure 9. The black square in figure represents the variation of the angular momentum during ignition. The red dotted line represents the fitting line of variation of the angular momentum during ignition.

The flywheel used by the satellite has a deviation of about 100 rpm near the 0 speed, so there may be some errors in the test results. However, through on-orbit attitude control tests of the micro-nano-satellite, we evaluated the capability of the laser micro-thruster for satellite attitude control and proved the applicability of the new technology and devices in the laser micro-thruster. In future work, we will carry out further on-orbit tests to evaluate the abilities of the laser micro-thruster in various scenarios, such as scenarios with long flight durations and large maneuvers. In addition, our team synchronously promoted the laser micro-thruster to carry out technical verification of orbit control capabilities with other micro- and nano-satellites, and related tasks are in the process of implementation.

5. Conclusions

In this paper, we presented the details of the SLP-1K laser micro-thruster, including the structural design, system composition, operating principle, and performance evaluation. The single impulse and average thrust of SLP-1K were measured based on ground measurement data. Then, it was launched into orbit to verify the actual on-orbit performance, and the actual on-orbit thrust of SLP-1K was obtained, which verified the feasibility of the laser micro-thruster for attitude control of micro- and nano-satellites. In conclusion, the SLP-1K laser micro-thruster developed in this study was the first to obtain on-orbit flight data; the results and performance data are of great significance for the field of micro-propulsion. The design, research and development process, and on-orbit test methods provide a reference for future development of laser micro-thrusters.

Author Contributions: Conceptualization, J.Y. and S.W.; methodology, J.Y. and H.C.; software, S.W.; validation, J.Y., Y.H. and S.W.; formal analysis, N.L. and C.X.; investigation, H.C.; resources, H.C.; data curation, H.C. and W.Z.; writing—original draft preparation, S.W., Y.H. and J.Y.; writing—review and editing, B.X., B.D., W.Z. and C.X.; visualization, B.D.; supervision, Y.H.; project administration, Y.H.; funding acquisition, Y.H. All authors have read and agreed to the published version of the manuscript.

Funding: This work was supported in part by the National Natural Science Foundation of China under Grant 11602304 and Grant 11502301 and Laser Propulsion and Applications State Key Laboratory Fund under Grant SKLLPA-202203.

Data Availability Statement: Data is unavailable due to privacy.

Conflicts of Interest: The authors declare no conflicts of interest. Spacety Co., Ltd. (Changsha) agreed to publish the paper.

References

1. Quinsac, G.; Segret, B.; Koppel, C.; Mosser, B. Attitude control: A key factor during the design of low-thrust propulsion for CubeSats. *Acta Astronaut.* **2020**, *176*, 40–51. [[CrossRef](#)]
2. Doncaster, B.; Williams, C.; Shulman, J. SpaceWorks' 2016 Nano/Microsatellite Market Forecast. In Proceedings of the 30th Annual AIAA/USU Conference on Small Satellites, Logan, UT, USA, 6–11 August 2016.
3. Lemmer, K. Propulsion for CubeSats. Propulsion for CubeSats. *Acta Astronaut.* **2017**, *134*, 231–243. [[CrossRef](#)]
4. Leomanni, M.; Garulli, A.; Giannitrapani, A.; Scortecchi, F. Propulsion options for very low Earth orbit microsatellites. *Acta Astronaut.* **2017**, *133*, 444–454. [[CrossRef](#)]
5. Edlerman, E.; Kronhaus, I. Analysis of Electric Propulsion Capabilities in Establishment and Keeping of Formation Flying Nanosatellites. In Proceedings of the 6th International Conference on Astrodynamics Tools and Techniques, Darmstadt, Germany, 14–17 March 2016.
6. Tardivel, S.; Klesh, A.T.; Campagnola, S. Technology Enabling Interplanetary Trajectories for Nanospacecraft. *J. Spacecr. Rocket.* **2018**, *55*, 95–105. [[CrossRef](#)]
7. Phipps, C.; Luke, J.; Helgeson, W. Laser space propulsion overview // Advanced Laser Technologies 2006. *SPIE* **2007**, *6606*, 15–26.
8. Phipps, C.; Luke, J.; Lippert, T.; Hauer, M.; Wokaun, A. Micropropulsion using laser ablation. *Appl. Phys. A* **2004**, *79*, 1385–1389. [[CrossRef](#)]
9. Zhang, Z.K.; Hang, G.R.; Qi, J.Y.; Zhang, Z.; Zhang, Z.; Liu, J.; Yang, W.; Tang, H. Design and fabrication of a full elastic sub-micron-Newton scale thrust measurement system for plasma micro thrusters. *Plasma Sci. Technol.* **2021**, *23*, 11. [[CrossRef](#)]
10. Yu, H.; Li, H.; Wang, Y.; Cui, L.; Liu, S.; Yang, J. Brief review on pulse laser propulsion. *Opt. Laser Technol.* **2018**, *100*, 57–74. [[CrossRef](#)]

11. Phipps, C.R.; Luke, J.R. Micro laser plasma thrusters for small satellites. In *High-Power Laser Ablation III*; SPIE: Bellingham, WA, USA, 2000; Volume 4065, pp. 801–809.
12. Phipps, C.; Luke, J.; Lippert, T.; Hauer, M.; Wokaun, A. Micropropulsion Using a Laser Ablation Jet. *J. Propuls. Power* **2004**, *20*, 1000–1011. [[CrossRef](#)]
13. Phipps, C.R. *Laser Ablation and Its Applications*; Springer: Berlin/Heidelberg, Germany, 2007; pp. 407–434.
14. Phipps, C.R.; Luke, J.R.; Helgeson, W. Liquid-fueled, Laser-powered, N-class thrust Space Engine with Variable Specific Impulse//AIP Conference Proceedings. *Am. Inst. Phys.* **2008**, *997*, 222–231.
15. Koizumi, H.; Inoue, T.; Arakawa, Y.; Nakano, M. Dual Propulsive Mode Microthruster Using a Diode Laser. *J. Propuls. Power* **2005**, *21*, 1133–1136. [[CrossRef](#)]
16. Nakano, M.; Ishikawa, T.; Wakabayashi, R. Laser propulsion technology on KKS-1 microsatellite. *Rev. Laser Eng.* **2011**, *39*, 34–40. [[CrossRef](#)]
17. Russian Information Agency. The Second Launch from “Vostochny” Spaceport. (In Russian). 2017. Available online: <https://ria.ru/science/20171128/1509717523.html> (accessed on 15 January 2020).
18. Gurin, A.; Kuvaev, K.; Loktionov, E.; Protasov, Y.; Sirenko, K.; Zakharov, V. First attempt of a laser thruster space flight test: Lost at launch. *Opt. Laser Technol.* **2019**, *120*, 105656. [[CrossRef](#)]
19. Jian, C. A High-Power Density Photonic Crystal Laser from the Institute of Semiconductors of the Chinese Academy of Sciences has been Launched with the Lijian 1. Available online: <https://dk.woofeelaser.com/info/the-high-power-density-photonic-crystal-laser-79127206.html> (accessed on 22 May 2023).
20. Sibó, W.; Bangdeng, D.; Baoyu, X.; Yanji, H.; Ying, W.; Baosheng, D.; Yongzan, Z.; Jiefei, Y.; Chenlin, L. Interface adhesion property and laser ablation performance of GAP-PET double-layer tape with plasma Treatment. *Nanomaterials* **2022**, *12*, 1827.
21. Guangyu W and Yanji, H. Modeling error analysis of micro—Impulse measurements. *J. Propuls. Technol.* **2009**, *30*, 509–512. (In Chinese)

Disclaimer/Publisher’s Note: The statements, opinions and data contained in all publications are solely those of the individual author(s) and contributor(s) and not of MDPI and/or the editor(s). MDPI and/or the editor(s) disclaim responsibility for any injury to people or property resulting from any ideas, methods, instructions or products referred to in the content.